Received: 23 July 2020 | Revised: 21 October 2020 | Accepted: 13 November 2020

DOI: 10.1111/adb.12995

ORIGINAL ARTICLE

Addiction Biology SSA WILEY

Regulation of GluA1 phosphorylation by *d*-amphetamine and methylphenidate in the cerebellum

Laura Cutando[1] | Emma Puighermanal[1,2] | Laia Castell[1] | Pauline Tarot[1] | Federica Bertaso[1] | Patricia Bonnavion[3] | Alban de Kerchove d'Exaerde[3] | Elsa Isingrini[4,5] | Micaela Galante[6] | Glenn Dallerac[6] | Vincent Pascoli[7] | Christian Lüscher[7] | Bruno Giros[4,5] | Emmanuel Valjent[1]

[1]IGF, University of Montpellier, CNRS, Inserm, Montpellier, France

[2]Neurosciences Institute, Department of Cell Biology, Physiology and Immunology, Autonomous University of Barcelona, Barcelona, Spain

[3]Laboratory of Neurophysiology, ULB Neuroscience Institute, Université Libre de Bruxelles (ULB), Brussels, Belgium

[4]Integrative Neuroscience and Cognition Center, University of Paris, CNRS, Paris, France

[5]Department of Psychiatry, Douglas Hospital, McGill University, Montreal, Quebec, Canada

[6]Pharmacologie et Biochimie de la Synapse, Institut des Neurosciences Paris-Saclay, University of Paris-Saclay, University of Paris-Sud, CNRS, UMR, Orsay, France

[7]Department of Basic Neurosciences, Medical Faculty, University of Geneva, Geneva, Switzerland

Correspondence
Emmanuel Valjent, IGF, Univ. Montpellier, CNRS, Inserm, F-34094 Montpellier, France.
Email: emmanuel.valjent@igf.cnrs.fr

Funding information
CIHR, Grant/Award Number: 201803PJT; Brain and Behavior Research Foundation; Agence nationale de la recherche, Grant/Award Number: DOPAFEAR; Agence nationale de la recherche, Grant/Award Number: EPITRACES; *La Marató de TV3 Fundació*, Grant/Award Number: #113-2016; *Fondation pour la Recherche Médicale*, Grant/Award Number: DEQ20160334919; Inserm

Abstract

Prescription stimulants, such as *d*-amphetamine or methylphenidate are used to treat suffering from attention-deficit hyperactivity disorder (ADHD). They potently release dopamine (DA) and norepinephrine (NE) and cause phosphorylation of the α-amino-3-hydroxy-5-methyl-4-isoxazolepropionic acid (AMPA) receptor subunit GluA1 in the striatum. Whether other brain regions are also affected remains elusive. Here, we demonstrate that *d*-amphetamine and methylphenidate increase phosphorylation at Ser845 (pS845-GluA1) in the membrane fraction of mouse cerebellum homogenate. We identify Bergmann glial cells as the source of pS845-GluA1 and demonstrate a requirement for intact NE release. Consequently, *d*-amphetamine-induced pS845-GluA1 was prevented by β1-adenoreceptor antagonist, whereas the blockade of DA D1 receptor had no effect. Together, these results indicate that NE regulates GluA1 phosphorylation in Bergmann glial cells in response to prescription stimulants.

KEYWORDS

Bergmann glial cells, cerebellar cortex, GluA1, monoaminergic system, prescription stimulants

Abbreviations: AC, adenylyl cylase; ADHD, attention-deficit hyperactivity disorder; AMPA, α-amino-3-hydroxy-5-methyl-4-isoxazolepropionic acid; BGCs, Bergmann glial cells; CC, cerebellar cortex; D1R, dopamine D1 receptor; DA, dopamine; *d*-amph, *d*-amphetamine; DAT, dopamine transporter; GluA1, AMPA subunit A1; HA, hemagglutinin; LC, locus coeruleus; Mph, methylphenidate; NE, norepinephrine; PC, Purkinje cell; PKA, protein kinase A; PKC, protein kinase C; SN, *substantia nigra*; TH, tyrosine hydroxylase; VMAT2, vesicular monoamine transporter 2; VTA, ventral tegmental area; β1-AR, beta-1-adrenergic receptors; β-AR, beta-adrenergic receptors.

1 | INTRODUCTION

Attention-deficit hyperactivity disorder (ADHD) is a neurodevelopmental disorder characterized by a myriad of symptoms including distractibility, hyperactivity and impulsivity.[1] Children and adults diagnosed for ADHD are generally treated with stimulant medications such as *d*-amphetamine (Adderrall®) and methylphenidate (Ritaline®). The drugs are also abused recreationally and can lead to addiction.[2] A comprehensive understanding of the molecular actions may allow refining ADHD therapy.

The main pharmacological effects of these drugs are the increase of extracellular concentrations of dopamine (DA) and norepinephrine (NE) in the striatum and the prefrontal cortex,[3,4] thought to increase alertness and attention[5] while at the same time hijack reward processing, motivation, motor and executive functions.[6] Given the widespread DA and NE projections throughout the central nervous system, stimulant-induced molecular adaptations may occur in other brain regions.

For example, dopaminergic and noradrenergic projections to the cerebellum arise from midbrain DA neurons (ventral tegmental area [VTA]/*substantia nigra* [SN] c) and hindbrain NE neurons (locus coeruleus [LC]).[7–9] They modulate the activity of both cerebellar neurons and glial cells, which express dopaminergic and adrenergic receptors. Although the cerebellum is not considered as a primary site of actions of stimulant medications, evidence indicates that these drugs alter cerebellar neuronal activity as well as monoamine turnover[10,11] and ameliorate some of the cerebellar abnormalities associated to ADHD symptoms.[12] However, the regulation of intracellular signaling events following stimulants exposure in the cerebellum remains elusive.

Phosphorylation is a posttranslational modification enabling the rapid functional regulation of many proteins. The GluA1 subunit of the glutamate α-amino-3-hydroxy-5-methyl-4-isoxazolepropionic acid (AMPA) receptor is an example of such process. GluA1 can be phosphorylated on two serine residues (pS845 and pS831) achieved by cAMP-dependent protein kinase A (PKA) at pS845 and by calcium/calmodulin-dependent (CaMKII) and protein kinase C (PKC) at pS831, respectively.[13] Phosphorylation of these two sites directly regulates surface trafficking of GluA1 and its interaction with intracellular proteins as well as electrophysiological properties of AMPA receptors.[13,14] Levels of GluA1 phosphorylation have been reported to be sensitive and modulated by stimulant exposure. For example, acute *d*-amphetamine and methylphenidate administration increases pS845-GluA1, but not pS831-GluA1, in both the striatum and the prefrontal cortex.[15,16] AMPA receptors are also widely expressed in the cerebellum.[17] Within cerebellar astrocytes, GluA1 is found only in Bergmann glial cells (BGCs).[18–20]

In this study, we probed the ability of *d*-amphetamine and methylphenidate to modulate GluA1 phosphorylation in BGCs. We also investigated the contribution of DA and NE transmission in the control of stimulants-induced GluA1 phosphorylation and determined the impact of repeated exposure to stimulant medications on these intracellular signaling events.

2 | MATERIALS AND METHODS

2.1 | Animals

Eight-week-old male C57BL/6 were purchased from Charles River Laboratories. The different transgenic mouse lines used are detailed in Table S1. Mice were housed under standardized conditions with a 12-h light/dark cycle, stable temperature (21 ± 2°C), controlled humidity (55 ± 10%), and food and water ad libitum. All experiments were in accordance with the guidelines of the French Agriculture and Forestry Ministry for handling animals (authorization number/license D34-172-13). Mice were arbitrarily assigned to pharmacological treatments. The number of animals used in each experiment is reported in the figure legends. No statistical methods were used to predetermine sample sizes, but they are comparable with those generally used in the field. For characterization experiments (immunofluorescence, polysome immunoprecipitation [IP], quantitative real-time polymerase chain reaction [qRT-PCR]) male and female mice were used. For Western blot analyses, only male mice were used.

2.2 | Drugs

(*d*)-Methylphenethylamine (*d*-amphetamine) sulfate salt, methylphenidate hydrochloride, cocaine, GBR12783, propranolol, and betaxolol were from Sigma-Aldrich (St. Louis, MO, USA). SCH23390 was from Tocris (Bristol, UK). All drugs were injected intraperitoneally (i.p.) in a body volume of 10 ml/kg and dissolved in 0.9% (w/v) NaCl (saline) except GBR12783, which was dissolved in H_2O. Tamoxifen was dissolved in sunflower oil/ethanol (10:1) to a final concentration of 10 mg/ml and administered i.p. in a volume of 10 ml/kg (100 mg/kg).

2.3 | Treatments

Acute pharmacological treatments were carried out with saline, *d*-amph (10 mg/kg), mph (15 mg/kg), cocaine (20 mg/kg) and GBR12783 (15 mg/kg). Mice were sacrificed 15 min after injections. The various antagonists were injected 30 min prior to saline, *d*-amph (10 mg/kg) or mph (15 mg/kg) injection. Propranolol and betaxolol were administered at 20 mg/kg; SCH-23390 at 0.1 mg/kg. For chronic treatments, saline, *d*-amph (10 mg/kg), and mph (15 mg/kg) were administered once per day during 5 days. Betaxolol (20 mg/kg) was administered 30 min prior to saline, *d*-amph (10 mg/kg), or mph (15 mg/kg) injection. Mice were killed 15 min after the fifth *d*-amph or mph administration. To induce the Cre expression in the *Gfap-Cre^{ERT2}::RiboTag* mice (here referred as *Gfap-RiboTag*), tamoxifen

(100 mg/kg) was administered during three consecutive days i.p. in a volume of 10 ml/kg.

2.4 | Stereotaxic injection in the VTA and the LC

Stereotaxic injections in the VTA of *Slc6a3-Cre* mice have been performed as previously described.[21] Six-week-old C57Bl6 *Dbh-Cre* mice were anesthetized in isoflurane (4.0% for induction, 0.5%–1.0% for maintenance) in oxygen (0.5 L/min) and mounted in a stereotaxic frame (Model 940, David Kopf Instruments). The skin on the head was shaved and aseptically prepared, and 2 mg/kg lidocaine infused subcutaneously at the incision site. A single longitudinal midline incision was made from the level of the lateral canthus of the eyes to the lambda skull suture. Injections were performed using a 30-gauge needle (Cooper's Needleworks Ltd) connected by phosphate-buffered saline (PBS) 0.01-M filled tubing to a 10-μl Hamilton syringe in an infusion pump (KDS 310 Plus Nano Legacy Syringe Pump, KD Scientific). Injections were performed at 0.1 μl/min, and the needle was left in situ for 15 min afterwards to allow diffusion. Injections were performed in LC (AP −5.4 mm from bregma skull suture, ML +/−1.2 mm, DV −3 mm from brain surface, 800 nl). Coordinates were based on the mouse brain atlas.[22] Animals received Cre-inducible recombinant AAV vector prepared by the viral vector core at the University of North Carolina (lot AV4311c, 3.6×10^{12} genome copies (gc)/ml) AAV2.5-EF1a-DIO-mCherry for anatomical tracing of LC NE neurons projections. Animals were allowed to recover in individual housing after surgery, and we awaited at least 8 to 12 weeks for transgene expression in terminals before being killed for histology.

2.5 | Tissue preparation and immunofluorescence

Tissue preparation and immunofluorescence were performed as previously described.[23] Mice were rapidly anesthetized with Euthasol® (360 mg/kg, i.p., TVM lab, France) and transcardially perfused with 4% (w/v) paraformaldehyde in 0.1-M sodium phosphate buffer (pH 7.5). Brains were post-fixed overnight in the same solution and stored at 4°C. Forty-micrometer thick sections were cut with a vibratome (Leica, France) and stored at −20°C in a solution containing 30% (v/v) ethylene glycol, 30% (v/v) glycerol and 0.1-M sodium phosphate buffer, until they were processed for immunofluorescence. Sagittal cerebellar sections were identified using a mouse brain atlas[22] and were processed as follows: free-floating sections were rinsed three times 10 min in Tris-buffered saline (TBS, 50-mM Tris–HCL, 150-mM NaCl, pH 7.5). After 20-min incubation in 0.1% (v/v) Triton X-100 in TBS, sections were rinsed in TBS again during 10 min and blocked for 1 h in a solution of 3% bovine serum albumin (BSA) in TBS. Cerebellar sections were then incubated 72 h at 4°C with the primary antibodies (Table S2) diluted in a TBS solution containing 1% BSA and 0.15% Triton X-100. Sections were rinsed three times for 10 min in TBS and incubated for 60 min with goat Cy3-coupled anti-rabbit (1:500, Thermo Fisher Scientific Cat# 10520), goat Alexa Fluor 594-coupled anti-chicken (1:400, Thermo Fisher Scientific Cat#A-11042), goat Alexa Fluor 488-coupled anti-chicken (1:500, Thermo Fisher Scientific Cat#A-11039), goat Alexa Fluor 488-coupled anti-mouse (1:500, Thermo Fisher Scientific Cat#A-11001), goat Alexa Fluor 488-coupled anti-rabbit (1:500, Life Technologies Cat#A-11034), goat Cy5-coupled anti-mouse (1:500, Thermo Fisher Scientific Cat#A-10524), goat Cy3-coupled anti-mouse (1:500, Jackson ImmunoResearch Cat#115–165-003), or goat Cy5-coupled anti-rabbit (1:500, Thermo Fisher Scientific, Cat#A10523) antibodies. Sections were rinsed for 10 min (twice) in TBS and twice in Tris buffer (0.25 M, pH 7.5) before mounting in DPX (Sigma-Aldrich). Confocal microscopy and image analysis were carried out at the Montpellier RIO Imaging Facility. Images covering the entire cerebellum and double-labeled images from each region of interest were acquired using sequential laser scanning confocal microscopy (Zeiss LSM780). Photomicrographs were obtained with the following band-pass and long-pass filter setting: Alexa Fluor 488/Cy2 (band-pass filter: 505–530), Cy3 (band-pass filter: 560–615) and Cy5 (long-pass filter 650). All parameters were held constant for all sections from the same experiment. Three to four slices per mouse were used in all immunofluorescence analyses (n = 2–3 mice per staining).

2.6 | Tissue collection and samples preparation for western blot analysis

Mice were killed by cervical dislocation, and the heads were immersed in liquid nitrogen for 4 s. The brains were then removed and sectioned on an aluminum block on ice, and the whole cerebellum was rapidly isolated from the brainstem. For Figure 2A, the whole cerebellum was sonicated in 300 μl of 10% sodium dodecyl sulfate (SDS) and boiled at 95°C for 10 min. For other figures, subcellular fractionation was performed after tissue collection as previously described.[24] In each experiment, samples from different animal groups, treatments, or brain regions were processed in parallel to minimize inter-assay variations.

2.7 | Western blot

Protein quantification and western blots were performed following the protocol previously described.[23] Following the manufacturer's instructions, protein contents for each sample were determined by BCA protein assay (Pierce) (Lot# RG235624; Thermo Scientific). Equal amounts of cerebellar lysates were mixed with denaturing 4× Laemmli loading buffer. Samples with equal amounts of total protein were separated in 11% SDS-polyacrylamide gel before electrophoretic transfer onto Immobilon-P membranes (#IPVH00010; Millipore). Membranes were cut horizontally at different molecular weights to be analyzed with different primary antibodies. Using 4% BSA in 0.1-M PBS, membranes were blocked for 45 min and then incubated for 2 h with the primary antibodies (Table S2). To detect the primary antibodies, horseradish peroxidase-conjugated antibodies (1:10,000) from Cell

Signaling Technology to rabbit (Cat# 7074S) or mouse (Cat#7076S) were used and visualized by enhanced chemiluminescence detection (Luminata Forte Western HRP Substrate; Millipore, Cat# WBWF0500). The optical density (OD) of the relevant immunoreactive bands was measured after acquisition on a ChemiDoc Touch Imaging System (Bio-Rad) controlled by Image Lab software version 3.0 (Bio-Rad). Representative cropped immunoblots for display were processed with Adobe Illustrator CS6. For quantitative purposes, the OD values of active phospho-specific antibodies were normalized to the detection of non-phospho-specific antibodies in the same sample and expressed as a percentage of control treatment or group. More specifically, in Figures 2A,C, 4C,D, 5G, and 6A, because the home-made stripping solution was not strong enough to ensure the removal of the first antibodies tested, the evaluation of pS845-GluA1 or p831-GluA1 and the total form GluA1 was performed in two different gels. The OD of phospho-sites and the OD of GluA1 were normalized gel to the OD of control proteins β-actin or GADPH in each gel. Therefore, the analysis of the OD was performed as follow: pS845-GluA1 or p831-GluA1/β-actin or GADPH (Gel 1) versus GluA1/β-actin or GADPH (Gel 2). In Figures 2B and 5D, GluA1 was evaluated after stripping of pS845-GluA1 or p831-GluA1. β-actin was assessed in the same gel. The analysis of the OD was performed as follows: pS845-GluA1 or p831-GluA1 versus GluA1/β-actin. Finally, in the Figure 6C OD of pS845-GluA1 was directly normalized to OD of GluA1. The number of samples and the statistical test used in each experiment are specified in the figure legends.

2.8 | Tissue collection for polysome IP

Three weeks after the tamoxifen administration, male and female *Gfap-RiboTag* mice were killed by cervical dislocation and the heads were immersed in liquid nitrogen for 4 s. The brains were then removed and sectioned on an aluminum block on ice, and the whole cerebellum was rapidly isolated from the stem brain. Then, cerebellar samples were kept at −80°C until they have been used to performed polysome IP.

2.9 | Polyribosome immunoprecipitation and RNA extraction

HA-tagged-ribosome immunoprecipitation in the cerebellum of *Gfap-RiboTag* mice was performed as it was previously described[25] using anti-HA antibody (5 μl/sample; BioLegend; Cat#901502) and magnetic beads (Invitrogen, #100.04D). Total RNA contained in the pellet fraction was extracted from ribosome-mRNA complexes using RNeasy Micro Kit (Qiagen; Cat#74004) and from the input fraction using the RNeasy Mini Kit (Qiagen; Cat#74104) following manufacturer's instructions. Quality and quantity of RNA samples were both assessed using the NanoDrop 1000 spectrophotometer. Between 5 and 9 biological replicates, each one composed of a pool of two mice, were used for qRT-PCR analysis (Figures 1E, 4B, 5E, and S5). For the RNA extraction in Figures 5C, 6B, 6D, and S4, we used the RNAeasy Mini Kit (Qiagen; Cat#74104) following the manufacturer's instruction.

2.10 | cDNA synthesis and qRT-PCR

After RNA extraction from pellet and the input fractions of CC *Gfap-RiboTag* mice, synthesis of cDNA was performed as it was previously described by using the SuperScript VILO cDNA synthesis kit (Invitrogen) in one cycle program consisting of 10 min at 25°C, 60 min at 42°C, 5 min at 25°C, and a final extension period of 5 min at 4°C. Resulting cDNA was used for qRT-PCR, using SYBR Green PCR master mix on the LC480 Real-Time PCR System (Roche) and the primer sequences reported in Table S3. Analysis was performed using LightCycler 480 Software (Roche). In Figures 1E, 3C, 4B, 5E, and S4, the immunoprecipitated mRNA (pellet fraction) was compared with the input fraction. Results are presented as linearized Ct-values and normalized to the housekeeping *Tbp* (WO 2018/134305 Al). ΔΔCT method was used to give the fold change. Five to nine biological replicates were used in these experiments. In Figures 5C and S4, results are presented as percentage of change of VMAT2-cKO mice compared with control mice for each gene tested and normalized to the housekeeping gene *Tbp*. In Figure 6, results are presented as percentage of change of chronic *d*-amphetamine or methylphenidate versus chronic saline for each gene tested and normalized to the housekeeping gene *Tbp*.

2.11 | Single-molecule fluorescent in situ hybridization

For the examination of targeted RNA within intact cells, in situ hybridization RNAscope® technology was used following the protocol described by the supplier. Mice were decapitated, and brains were frozen immediately on dry ice for 5 min and stored at −80°C. Brains were then sectioned at −17°C with a cryostat at 14 μm and mounted onto SuperFrost Ultra Plus slides (Thermo Scientific; Cat# J4800AMNZ). Coronal cerebellar sections were collected from bregma −5.80 and −6.80 mm. Probes for *Adrb1* (ACDBio; Mm-adrb1-C1 Cat# 449761) and *Gfap* (ACDBio; Mm-gfap-C3 Cat#313211-C3) were used with the RNAscope Fluorescent Multiplex Kit (ACDBio; Cat# 320850) as described by the supplier. Slides were counterstained for DAPI and mounted with ProLong Diamond Antifade Mountant (Invitrogen; Cat# P36961).

2.12 | Statistical analyses

GraphPad Prism v6.0 software was used for statistical analyses. For normally distributed data, Student's *t* test was used. Multiple comparisons were performed by one-way or two-way ANOVA followed by Tukey's post-hoc analyses. All data are presented as mean ± SEM, and

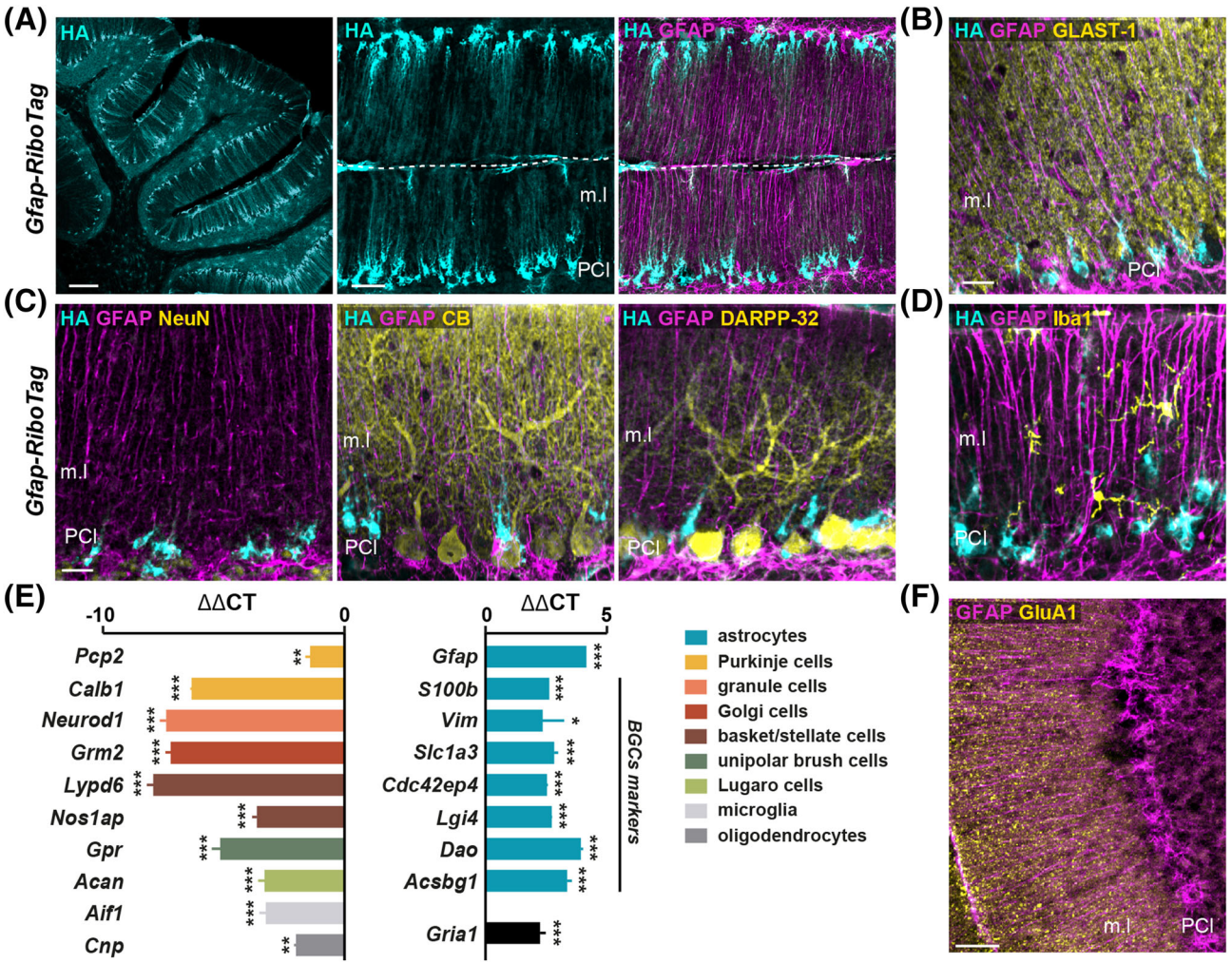

FIGURE 1 GluA1 are expressed in cerebellar astrocytes in adult mice. (A) Sagittal section from *Gfap-RiboTag* mice stained with hemagglutinin (HA) (cyan) showing the distribution of GFAP-expressing cells in the cerebellar cortex. Scale bar: 400 μm (left image). Double immunofluorescence for HA (cyan) and GFAP (magenta). Scale bar: 62 μm (right images). (B–D) Triple immunofluorescence for HA (cyan), GFAP (magenta) and the astrocytic marker GLAST-1 (yellow) (B), the neuronal markers NeuN, Calbindin-D28k (CB), and DARPP-32 (yellow) (C), and the microglial marker Iba1 (D). Scale bar: 15 μm. (E) Validation by quantitative real-time polymerase chain reaction (qRT-PCR) (ΔΔCT) of the enrichment of glial markers (cyan) and depletion of transcripts encoding Purkinje cell (PC), interneurons, oligodendrocyte, and microglial markers after HA-immunoprecipitation from cerebellar extract compared with the input fraction (n = 5–6 pooled samples of two mice per pool). All genes were normalized to *Tbp*. Data were analyzed by two-sided t test. $^{*}p < 0.05$; $^{**}p < 0.01$; $^{***}p < 0.001$. (F) Double immunofluorescence in the cerebellar cortex for GluA1 (yellow) and GFAP (magenta). Scale bar: 60 μm. Note the expression of GluA1 in BGCs of the m.l. scale bar: 100 μm. PCl, Purkinje cell layer; g.l, granular layer; m.l, molecular layer. For detailed statistics, see Table S4

statistical significance was accepted at 5% level. $^{*}p < 0.05$, $^{**}p < 0.01$, $^{***}p < 0.001$. All the statistics are presented in the Table S4.

3 | RESULTS

3.1 | GluA1 is expressed in Bergmann glial cells in the adult mouse cerebellum

To confirm the preferential expression of GluA1 subunit of AMPA receptors in BGCs in the adult mouse cerebellum,[26] we took advantage of the RiboTag methodology to isolate *Gria1* transcripts from BGCs. We first generated *Gfap-RiboTag* mice, which express the ribosomal protein Rpl22 tagged with hemagglutinin (HA) exclusively in astrocytes (Figure 1). Indeed, immunofluorescence analyses revealed that the vast majority of HA-positive cells had the typical morphology of BGCs with their cell bodies located in the PC layer and radial processes crossing the entire molecular layer. Moreover, these HA-positive cells co-localized with the astrocytic marker GFAP as well as with the glial glutamate/aspartate transporter GLAST-1 confirming their astrocytic nature (Figure 1A,B). In contrast, no co-localization was observed with neuronal (NeuN), Purkinje cells (PCs) (Calbindin-D28k, DARPP-32) or microglial (Iba1) markers (Figure 1C,D). The specificity of *Gfap-RiboTag* mice was further validated by assessing

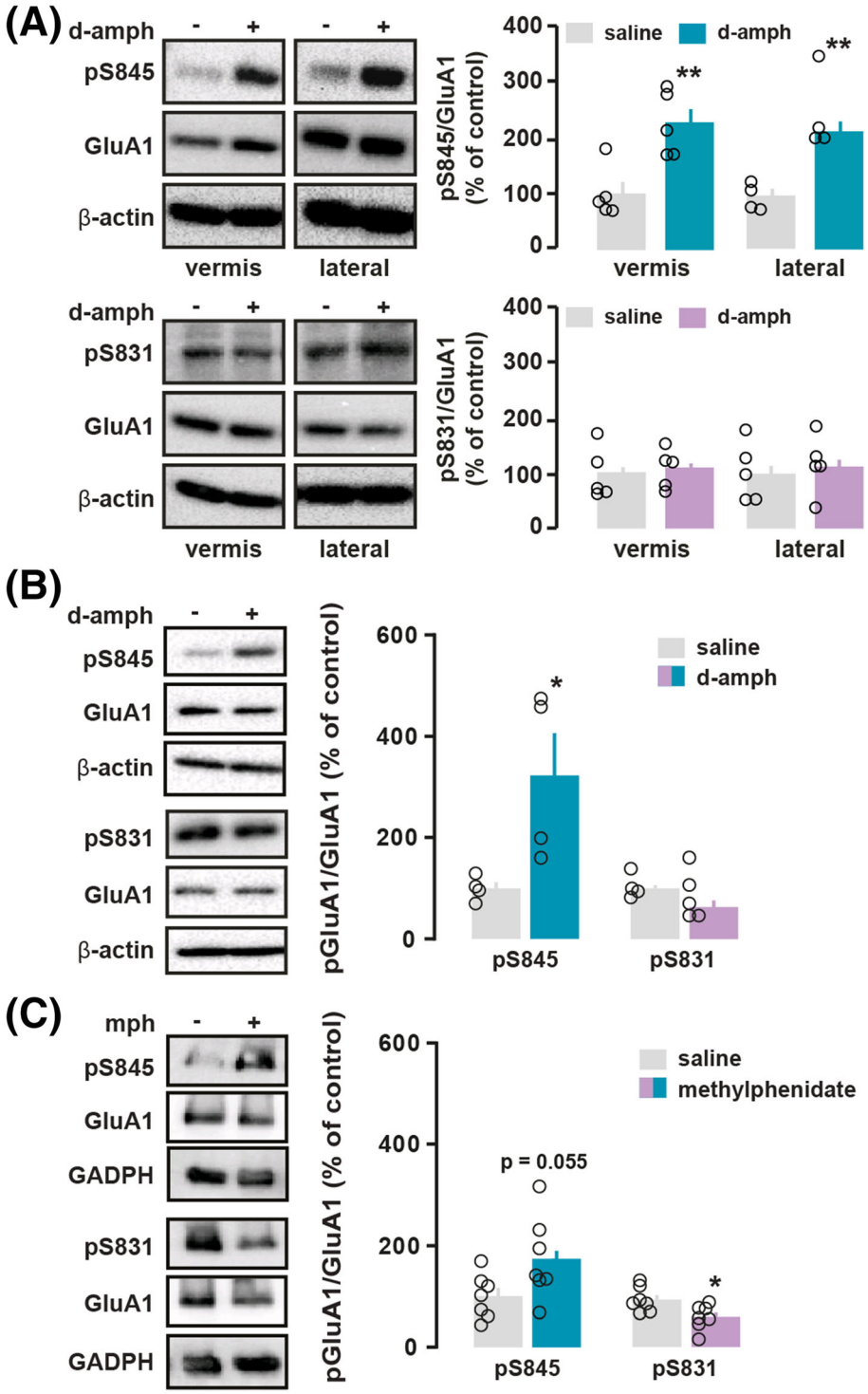

FIGURE 2 Acute psychostimulant administration increases S845 GluA1 phosphorylation in the cerebellum. (A) Representative immunoblots (left) and quantification (right) of GluA1 phosphorylation at S845 (pS845-GluA1) (top) or at S831 (pS831-GluA1) (bottom) in the vermis and lateral hemispheres of C57/Bl6 mice 15 min after a single administration of saline or *d*-amphetamine (*d*-amph, 10 mg/kg). Phosphorylated forms of GluA1 were normalized to unphosphorylated GluA1. β-actin was used as housekeeping protein. Data are expressed as percentage of saline group (n = 4–5 mice per group for vermis and lateral). Data are presented as mean ± SEM and analyzed by two-sided t test. $^{**}p < 0.01$. (B,C) Representative immunoblots (left) and quantification (right) of GluA1 phosphorylation at S845 (pS845-GluA1) (top) or at S831 (pS831-GluA1) (bottom) in membrane cerebellar extracts of C57/Bl6 mice 15 min after a single administration of saline, *d*-amphetamine (*d*-amph, 10 mg/kg) (B) or methylphenidate (mph, 15 mg/kg) (C). Phosphorylated forms of GluA1 were normalized to unphosphorylated GluA1. β-actin (B) and GAPDH (C) were used as housekeeping proteins. Data are expressed as percentage of saline group (n = 4–5 mice per group for *d*-amph, n = 7 mice per group for mph). Data are presented as means ± SEM and analyzed by two-sided t test. $^{*}p < 0.05$. For detailed statistics, see Table S4

the relative enrichment of astrocytic transcripts from mRNAs isolated after HA-immunoprecipitation on cerebellar extracts (Figure S1). As expected, qRT-PCR analyses revealed the enriched expression of several BGCs markers (*Gfap*, *S100b*, *Vim*, *Slc1a3*, *Cdc42ep4*, *Lgi4*, *Dao*, and *Acsbg1*)[27] in the pellet fraction compared with the input fraction (Figure 1E). In contrast, transcripts that molecularly defined PC (*Pcp2* and *Calb1*), granule cells (*Neurod1*), Golgi cells (*Grm2*), unipolar brush cells (*Grp*), Lugaro cells (*Acan*), GABAergic interneurons (*Lypd6* and *Nos1ap*), microglia (*Aif1*), and oligodendrocytes (*Cnp*) were all depleted (Figure 1E). In this *Gfap-RiboTag* mouse model, qRT-PCR analysis revealed that *Gria1* transcripts were enriched after HA-immunoprecipitation (Figure 1E). The preferential expression of GluA1 in the molecular layer of the cerebellar cortex was confirmed by immunofluorescence (Figure 1F). Altogether, these results confirmed previous work revealing that GluA1 is preferentially expressed in BGCs in the adult mouse cerebellum.[17]

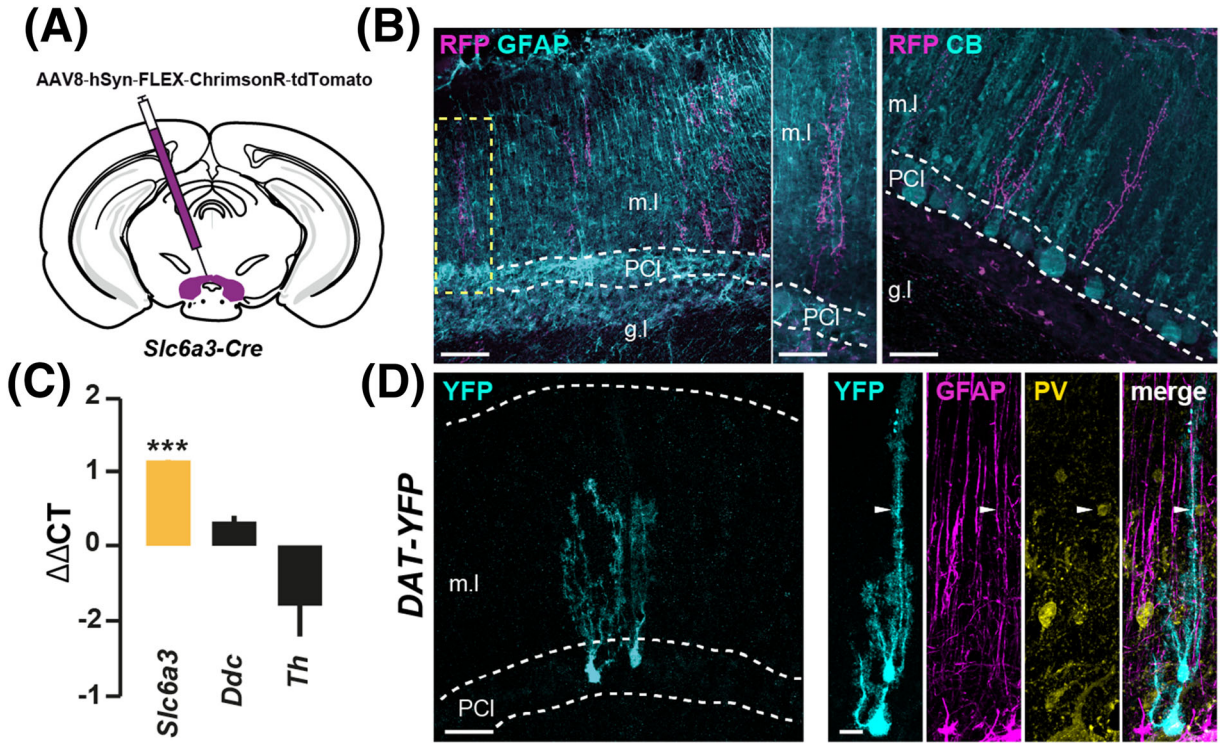

FIGURE 3 Sources of dopamine in the cerebellar cortex. (A) Scheme of Cre-dependent AAV8-hSyn-FLEX-ChrimsonR-tdTomato injection in the ventral tegmental area (VTA) of *Slc6a3-Cre* mice. (B) Double immunofluorescence for red fluorescent protein (RFP) (magenta), GFAP (cyan) (left) and calbindin-D28k (CB) (right) identifying RFP-expressing dopamine VTA neuron axons positive fibers in the cerebellar cortex. Note the orientation of RFP-positive fibers paralleling the BGCs. Scale bars: 60 μm (left), 15 μm (middle), 30 μm (right). (C) Quantitative real-time polymerase chain reaction (qRT-PCR) analysis of *Slc6a3*, *Th*, and *Ddc* transcripts in cerebellar extracts from *Gfap-RiboTag* mice after HA-immunoprecipitation. All genes were normalized to *Tbp*. Data are presented as the fold change comparing the pellet fraction versus the input (n = 4–5 pooled samples of two mice per pool). Data were analyzed by two-sided t test. ***$p < 0.001$. (D) Triple immunofluorescence for GFP (cyan), GFAP (magenta) and parvalbumin (PV; yellow) in the cerebellar cortex of *Slc6a3-Cre* mice crossed with the reporter mouse line *ROSA26-YFP* (*DAT-YFP*). White arrowhead indicates YFP-positive protrusion co-marked with GFAP. Scale bars: 30 and 10 μm. PCl, Purkinje cell layer; g.l, granular layer; m.l, molecular layer. For detailed, statistics see Table S4

3.2 | *d*-Amphetamine and methylphenidate increase GluA1 phosphorylation at serine 845 in the cerebellum

Acute administration of psychostimulant drugs, such as cocaine or *d*-amphetamine triggers a rapid increase of GluA1 phosphorylation at serine 845 (pS845-GluA1) in the striatum and prefrontal cortex.[16,28,29] To evaluate whether psychostimulants could produce similar effects in the cerebellum, C57/Bl6 mice were treated with *d*-amphetamine (10 mg/kg) and pS845-GluA1 was examined by western blot in both the vermis and the lateral lobes of the cerebellum (Figure 2). Acute *d*-amphetamine administration, which produced hyperlocomotion and stereotypies within 15 min after injection,[16] caused a rapid increase of pS845-GluA1 levels in the cerebellar vermis and lateral cerebellar hemispheres (Figure 2A). This effect was not accompanied by significant changes in the levels of total GluA1 detected with an antibody recognizing both the phosphorylated and unphosphorylated forms of GluA1 (Figure 2A). Moreover, subcellular fractionation of cerebellar lysates from mice injected with saline or *d*-amphetamine showed that pS845-GluA1 increases specifically in the membrane compartment (Figure 2B). In contrast, acute *d*-amphetamine failed to regulate GluA1 phosphorylation at serine 831 (pS831-GluA1) (Figure 2A,B). Similarly, an increase of pS845-GluA1 (p = 0.055) was observed in mice administered with methylphenidate (15 mg/kg), a psychostimulant drug commonly used for the treatment of ADHD (Figure 2C).[30] Interestingly, a significant decrease of pS831-GluA1 was observed in the membrane fraction of methylphenidate-treated mice (Figure 2C). Altogether, these results indicate that acute *d*-amphetamine or methylphenidate administration selectively enhances GluA1 phosphorylation at serine 845 which most likely occurred in BGCs.

3.3 | Regulation of pS845-GluA1 in BGCs in response to *d*-amphetamine is independent from cerebellar DA signaling

d-Amphetamine increases the extracellular concentration of DA availability in various brain areas.[31] We therefore conducted a series of experiments to determine whether DA signaling participates to the

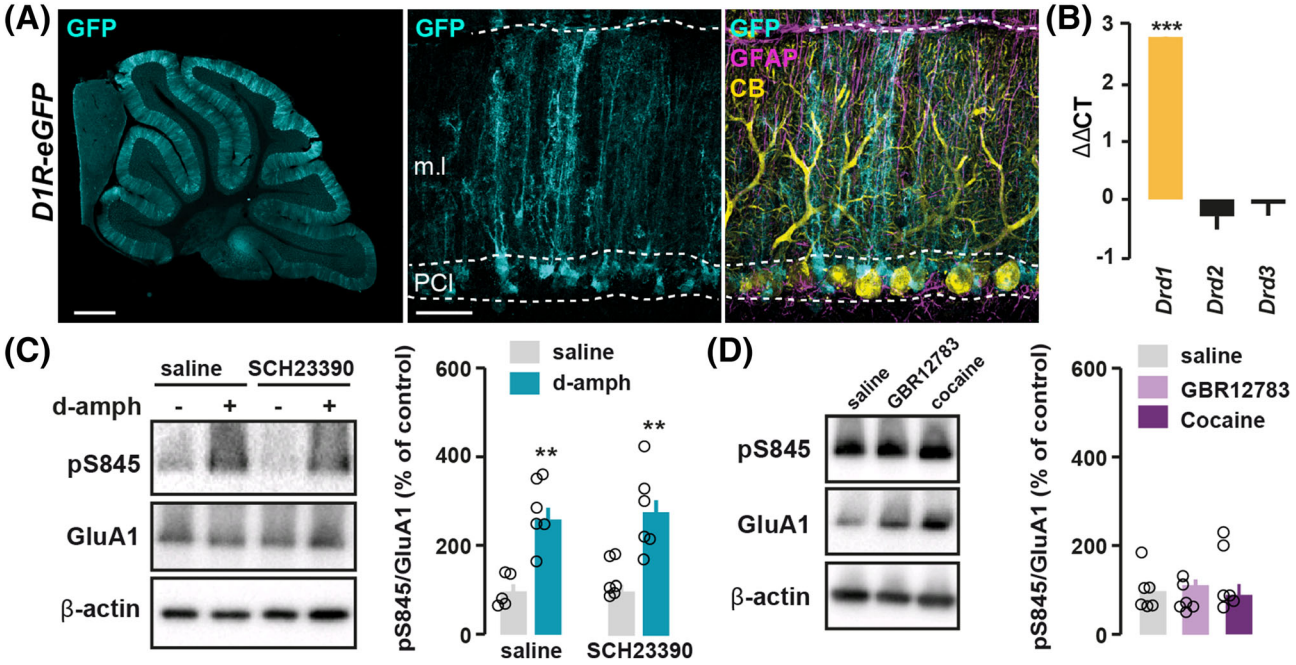

FIGURE 4 *d*-Amphetamine-induced GluA1 phosphorylation in Bergmann glial cells (BGCs) does not require D1R activation. (A) Sagittal section from *D1R-eGFP* mice stained with GFP (cyan) showing the distribution of D1R-expressing cells in the cerebellar cortex. Scale bar: 1 mm (left image). Triple immunofluorescence for GFP (cyan), GFAP (magenta), and calbindin-D28k (CB, yellow) (right images). Scale bar: 30 μm. (B) Quantitative real-time polymerase chain reaction (qRT-PCR) analysis of *Drd1*, *Drd2*, and *Drd3* transcripts in cerebellar extracts from *Gfap-RiboTag* mice after hemagglutinin (HA)-immunoprecipitation. All genes were normalized to *Tbp*. Data are presented as the fold change comparing the pellet fraction versus the input (n = 4–5 pooled samples of two mice per pool). Data were analyzed by two-sided t test. $^{***}p < 0.001$. (C) Representative immunoblots (left) and quantification (right) of GluA1 phosphorylation at S845 (pS845-GluA1) in the cerebellum of C57/Bl6 mice pretreated with the D1R/D5R antagonist, SCH23390 (0.1 mg/kg), 30 min prior to saline or *d*-amphetamine (10 mg/kg) administration. Phosphorylated forms of GluA1 were normalized to unphosphorylated GluA1. β-actin was used as housekeeping protein. Data are expressed as percentage of saline group (n = 5–6 mice per group). Data are presented as means ± SEM and analyzed by one-way ANOVA followed by Tukey post-hoc comparisons test. $^{**}p < 0.01$. (d) Representative immunoblots (left) and quantification (right) of GluA1 phosphorylation at S845 (pS845-GluA1) in the cerebellum of C57/Bl6 mice administered with saline, GBR12783 (15 mg/kg) and cocaine (20 mg/kg). Phosphorylated forms of GluA1 were normalized to unphosphorylated GluA1. β-actin was used as housekeeping protein. Data are expressed as percentage of saline group (n = 6 mice per group). Data are presented as mean ± SEM and analyzed by one-way ANOVA followed by Tukey post-hoc comparisons test. PCl, Purkinje cell layer; g.l, granular layer; m.l, molecular layer. For detailed statistics, see Table S4

regulation of pS845-GluA1 by *d*-amphetamine in the cerebellum. Immunofluorescence analyses revealed the presence of a dense lattice of TH-positive fibers and a strong VMAT2 immunoreactivity in the molecular layer suggesting that DA could be potentially released in the cerebellar cortex (Figure S2A,B). We first asked whether the VTA/SN constitute a source of dopaminergic fibers in the cerebellar cortex. To do so, midbrain DA axons were anterogradely labeled by injecting a Cre-dependent virus (AAV8-hSyn-FLEX-ChrimsonR-tdTomato) in the VTA/SN of *Slc6a3-Cre* mice (Figure S3), expressing the Cre recombinase under the promotor of the DA transporter (DAT) (Figure 3A). Viral transduction of midbrain DAT-positive neurons resulted in sparse axonal labeling in the PC and molecular layers detected using an antibody directed against the red fluorescent protein (RFP) (Figures 3B and S3). In the molecular layer RFP-positive fibers are oriented in the same axis of PC being in close proximity of BGCs identified using anti-GFAP antibody (Figure 3B). These results indicate that midbrain constitutes a potential source of dopaminergic input for the cerebellum.

In various brain regions, astrocytes express, although at low levels, transcripts encoding proteins involved DA metabolism. We therefore evaluated the expression of transcripts encoding enzymes involved in DA biosynthesis (*Ddc*, *Th*) as well as the DA transporter DAT (*Slc6a3*) among mRNAs isolated after HA-immunoprecipitation in cerebellar extracts of *Gfap-RiboTag* mice (Figure 3C). Our qRT-PCR analysis revealed that the expression of *Slc6a3* was enriched in cerebellar GFAP-positive cells (Figure 3C). In contrast, no changes were observed for *Th* and *Ddc* transcripts, which encode for the tyrosine hydroxylase and the aromatic l-amino acid decarboxylase, respectively (Figure 3C). The presence of DAT in BGCs was further supported by the analysis of YFP expression in the cerebellar cortex of *DAT-YFP* mice (Figure 3D). Thus, sparse cerebellar YFP-expressing cells, which displayed typical BGCs morphology, co-expressed the astrocytic marker GFAP but not the GABAergic marker PV (Figure 3D). These findings indicate that DAT is expressed by a fraction of BGCs raising the possibility that BGCs reuptake DA in the cerebellum. Altogether, our results identify at least two potential sites through which DA

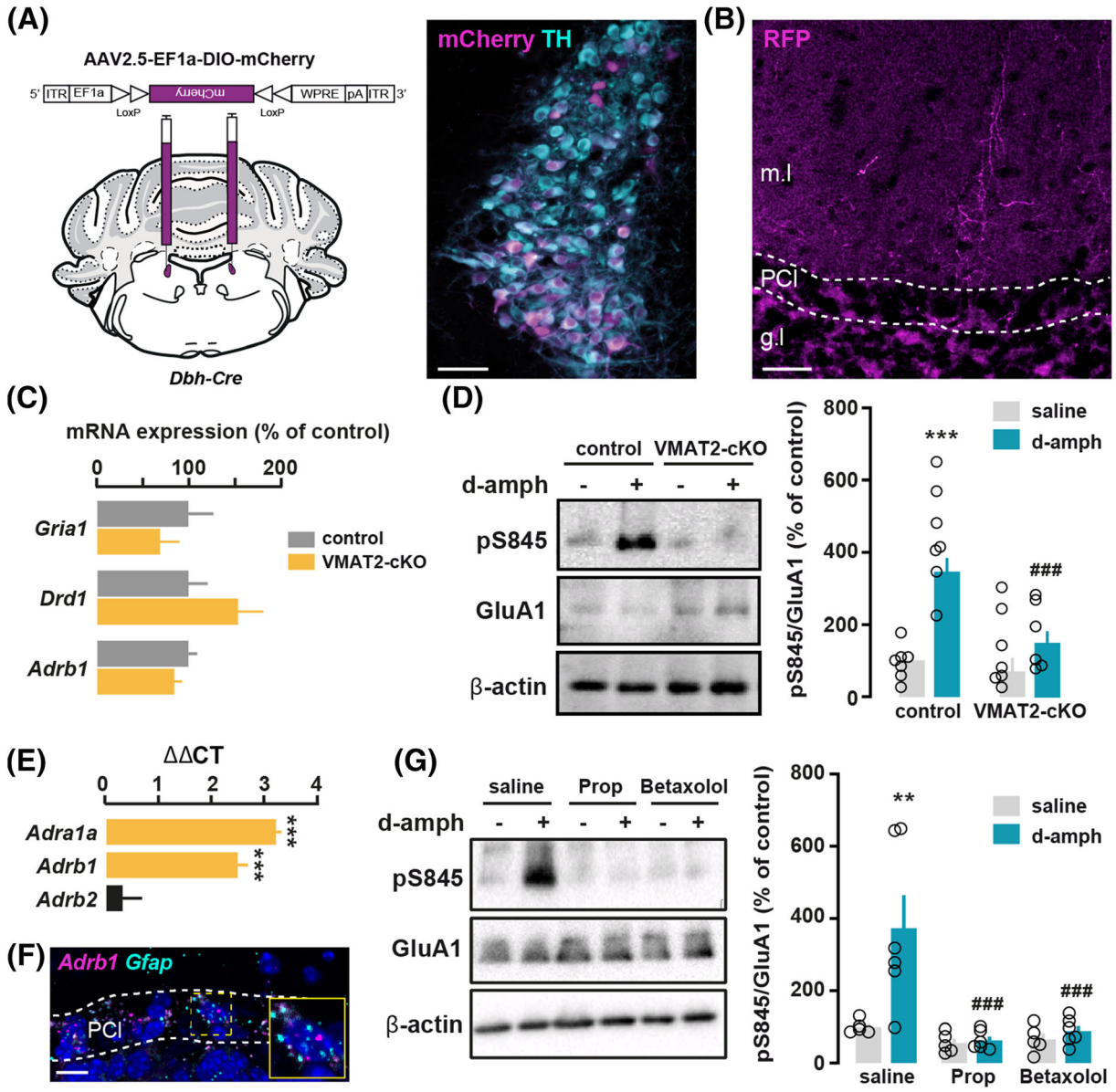

FIGURE 5 *d*-Amphetamine-induced p845-GluA1 requires intact norepinephrine (NE) transmission and β1-AR activation. (A) Scheme of Cre-dependent AAV2.5-EF1a-DIO-mCherry injection in the LC of *Dbh-Cre* mice and representative images of transduced DBH neurons expressing mCherry (magenta) and TH (cyan). Scale bar: 50 μm. (B) Red fluorescent protein (RFP)-expressing NE LC neuron axons positive fibers in the cerebellar cortex. Scale bar: 30 μm. (C) Expression of *Gria1*, *Drd1*, and *Adrb1* transcripts in cerebellar extracts of control and VMAT2-cKO mice. All genes were normalized to *Tbp*. Data are expressed as percentage of control (n = 7 mice). Results are represented as mean ± SEM. Data were analyzed by two-sided t test. (D) Representative (right) and quantification (right) of GluA1 phosphorylation at S845 in the cerebellar extracts of control and VMAT2-cKO mice treated with saline or *d*-amphetamine (10 mg/kg). β-actin was used as housekeeping protein. Data are expressed as a percentage of control mice treated with saline (n = 6–7 mice per group). Results are represented as mean ± SEM and analyzed by two-way ANOVA followed by Bonferroni's post-hoc comparisons. (E) Quantitative real-time polymerase chain reaction (qRT-PCR) analysis of *Adrb1*, *Adrb2*, and *Adra1a* transcripts in cerebellar extracts from *Gfap-RiboTag* mice after hemagglutinin (HA)-immunoprecipitation. All genes were normalized to *Tbp*. Data are presented as the fold change comparing the pellet fraction versus the input (n = 5–6 pooled samples of two mice per pool). Data were analyzed by two-sided t test. ***p < 0.001. (F) Single-molecule fluorescent in situ hybridization for *Adrb1* (magenta) and *Gfap* (cyan) mRNAs in the cerebellar cortex. The slide was counterstained with DAPI (blue). Note that *Adrb1* mRNAs are preferentially expressed in astrocytes in the PC layer most likely corresponding to somas of BGCs. Scale bar: 15 μm. (G) Representative (right) and quantification (right) of GluR1 phosphorylation at S845 in the cerebellar extracts of C57/Bl6 mice pretreated with the β1/2-AR antagonist propranolol (20 mg/kg) and β1-AR antagonist betaxolol (20 mg/kg), respectively, 30 min prior to saline or *d*-amphetamine (10 mg/kg) administration. Phosphorylated forms of GluA1 were normalized to unphosphorylated GluA1. β-actin was used as housekeeping protein. Data are expressed as a percentage of control mice treated with saline (n = 5–6 mice per group). Results are represented as mean ± SEM and analyzed by one-way ANOVA followed by Tukey's post-hoc comparisons. **p < 0.01 saline versus *d*-amph, ###p < 0.001 sal/*d*-amph versus drug/*d*-amph. PCl, Purkinje cell layer; g.l, granular layer; m.l, molecular layer. For detailed statistics, see Table S4

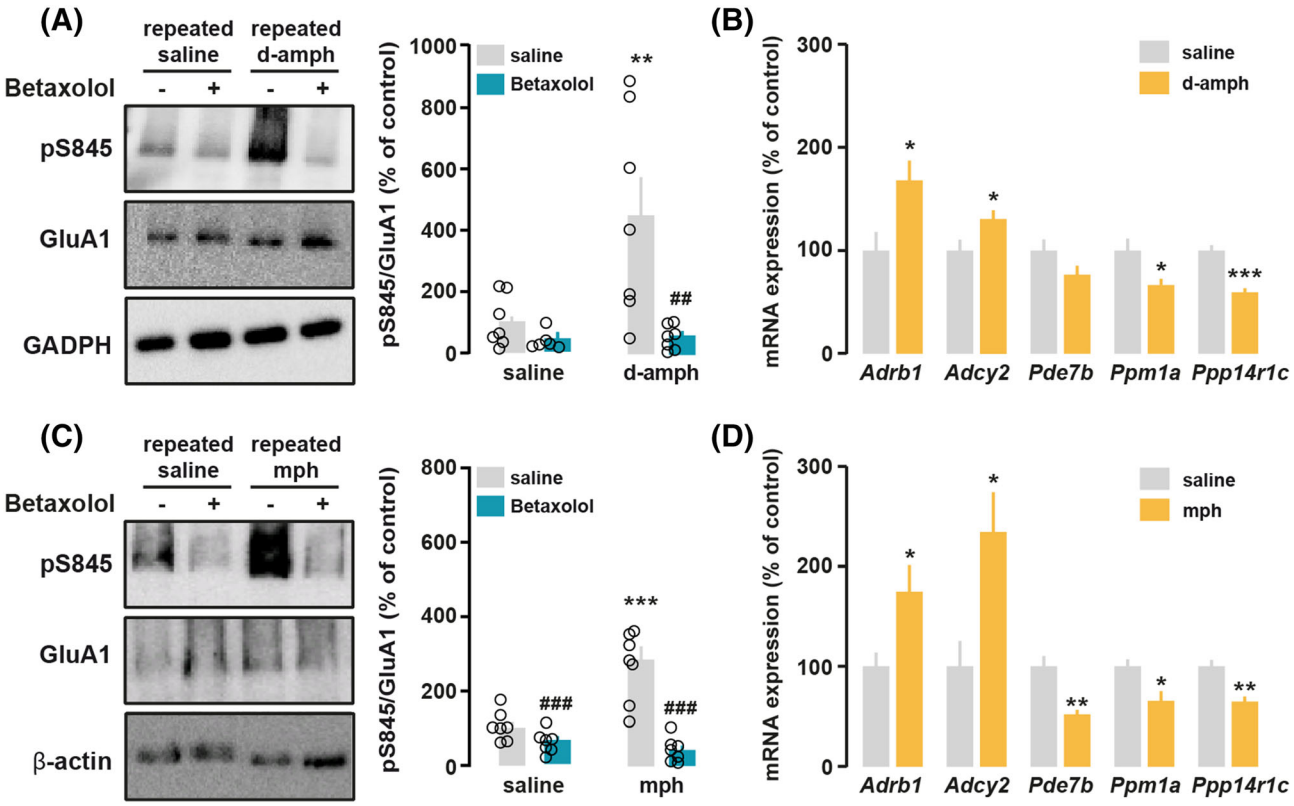

FIGURE 6 Effect of repeated exposure to *d*-amphetamine and methylphenidate on pS845-GluA1 in the cerebellum. (A) Representative immunoblots (left) and quantification (right) of GluA1 phosphorylation at S845 (pS845-GluA1) in the cerebellum of C57/Bl6 mice pretreated with betaxolol (20 mg/kg), 30 min prior to each injection of saline or *d*-amphetamine (10 mg/kg, 1 injection per day during 5 days). Phosphorylated forms of GluA1 were normalized to unphosphorylated GluA1. GAPDH was used as housekeeping protein. Data are expressed as percentage of saline group (n = 6–7 mice per group). Data are presented as mean ± SEM and analyzed by one-way ANOVA followed by Tukey post-hoc comparisons post. $^{**}p < 0.01$ saline versus *d*-amph, $\#\#p < 0.01$ saline versus betaxolol. (B) Comparison of the expression level of BG-enriched transcripts between mice repeatedly administered with saline or *d*-amphetamine. All genes analyzed by quantitative real-time polymerase chain reaction (qRT-PCR) were normalized to *Tbp*. Data are presented as mean ± SEM and analyzed by two-sided t test. $^{*}p < 0.05$, $^{***}p < 0.001$. (C) Same analyses as in (A) performed in methylphenidate-treated mice. Data are expressed as percentage of saline group (n = 6–7 mice per group). Data are presented as mean ± SEM and analyzed by one-way ANOVA followed by Tukey post-hoc comparisons post. $^{***}p < 0.001$ saline versus *d*-amph, $\#\#\#p < 0.001$ saline versus betaxolol. (D) Same analyses as in (C) performed in methylphenidate-treated mice. $^{*}p < 0.05$, $^{**}p < 0.01$. For detailed statistics, see Table S4

could be released and possibly participate to the regulation of pS845-GluA1.

In the striatum, *d*-amphetamine-induced pS845-GluA1 depends on cAMP-dependent protein kinase (PKA) activation downstream the stimulation of DA D1 receptors (D1R).[28,29] Despite early evidence suggesting the presence of D1R in the molecular layer of the cerebellum,[32] the cellular identity of D1R-expressing cells in the cerebellar cortex remains largely unknown. To address this issue, we analyzed the distribution of GFP-positive cells in the cerebellar cortex of *D1R-eGFP* mice (Figure 4). In all the lobules, a strong GFP labeling was found in the molecular layer of the cerebellar cortex (Figure 4A). Detailed analysis revealed that GFP-positive cells expressed GFAP, a marker of astrocytes, presumably corresponding to BGCs, but not the PC marker CB (Figure 4A). The presence of D1R in BGCs was further supported by the enrichment of *Drd1* transcripts among the mRNAs isolated following HA-immunoprecipitation in cerebellar extracts of *Gfap-RiboTag* mice (Figure 4B). In contrast, no differences were observed for *Drd2* and *Drd3* transcripts (Figure 4B). Together, these results indicate that D1R are expressed in BGCs.

To assess whether D1R participates to the regulation of GluA1 phosphorylation induced by *d*-amphetamine in BGCs, C57/Bl6 mice were administered with SCH23390 (0.1 mg/kg), a D1R/D5R-selective antagonist, 30 min prior the injection of *d*-amphetamine or saline. As shown in Figure 4, blockade of D1R/D5R had no effect on the basal or increased GluA1 phosphorylation at S845 induced by *d*-amphetamine measured in membrane fractions (Figure 4C). These results prompt us to hypothesize that DA is not involved in GluA1 regulation in BGCs. We therefore tested whether increasing the extracellular concentration of DA was sufficient to trigger pS845-GluA1 in the cerebellum. To do so, we measured the effect of cocaine (20 mg/kg) and GBR12783 (15 mg/kg), a selective DA reuptake inhibitor, on the phosphorylation of GluA1 at S845.

Although both drugs enhanced locomotor activity 15 min after administration,[33] they failed to increase pS845-GluA1 in BGCs (Figure 4D). Similar results were obtained following the acute administration of the D1R/D5R agonist, SKF81297 (data not shown). Altogether, our findings indicate that *d*-amphetamine-induced GluA1 phosphorylation at S845 in BGCs does not involve DA transmission and D1R/D5R stimulation, suggesting a decoupling of cAMP/PKA to D1R/D5R in BGCs.

3.4 | *d*-Amphetamine-induced increase of pS845-GluA1 requires noradrenergic transmission

In addition to its ability to release DA, *d*-amphetamine is also a potent releaser of NE.[5] We therefore examined whether the cerebellar cortex received noradrenergic-projecting neurons from the LC, the major noradrenergic nucleus of the brain. To selectively label hindbrain NE axons, we injected a Cre-dependent virus (AAV2.5-EF1a-DIO-mCherry) in the LC of mice expressing the Cre-recombinase under the DA β-hydroxylase promoter (*Dbh-Cre* mice) (Figure 5A). As shown in Figure 5, red fluorescent protein (RFP)-positive fibers were detected in the PC and molecular layers indicating that NE neurons from the LC constitute a source of noradrenergic input for the cerebellum (Figure 5B).

We investigated whether the noradrenergic transmission was involved in the increased pS845-GluA1 induced by *d*-amphetamine administration. To address this issue, we used brain NE-depleted conditional knock-out mice previously generated by crossing the *Dbh-Cre* mouse line with *Slc18a2*$^{loxP/loxP}$ mice (VMAT2-cKO).[34] As revealed by qRT-PCR analysis performed on cerebellar extracts, deletion of *Slc18a2* in DBH neurons neither altered level of transcripts encoding receptors (*Drd1*, *Drd2*, *Drd3*, *Adrb1*, *Adrb2*, and *Adra1a*) transporters (*Slc6a3* and *Slc6a2*), and enzymes involved in catecholamine biosynthesis (*Ddc* and *Th*) and degradation (*Comt*, *Maoa*, and *Maob*), nor changed the expression of *Gria1* transcripts (Figures 5C and S4). In addition, no changes were detected in the expression of transcriptsmenriched in glial cells including BGCs (*Gfap*, *Itgam*, *Aif1*, *Apq4*, and *Kcnj10*) and PC (*Gria2*). We then measured *d*-amphetamine-induced pS845-GluA1 in VMAT2-cKO. While cerebellar GluA1 expression was unaffected by the deletion of *Slc18a2* in the DBH neurons, the increase of pS845-GluA1 observed following *d*-amphetamine administration was totally abolished in VMAT2-cKO (Figure 5D). These results indicate that noradrenergic transmission is necessary for the regulation of GluA1 phosphorylation by *d*-amphetamine in BGCs.

We next investigated whether *d*-amphetamine-induced PKA-dependent GluA1 phosphorylation in BGCs required β-Adrenergic receptors (β-AR) that, upon agonist activation, stimulate the cAMP/PKA pathway.[35] Using mRNAs isolated after HA-immunoprecipitation in cerebellar extracts of *Gfap-RiboTag* mice, we determined the relative abundance of *Adrb1* and *Adrb2* transcripts encoding β1-AR and β2-AR, respectively (Figure 5E). Our analysis revealed that *Adrb1*, but not *Adrb2*, transcripts were significantly enriched in cerebellar GFAP-positive cells (Figure 5E). Of note, *Adra1a* transcripts encoding α1a-AR, which are highly expressed in BGCs,[36] were also detected after HA-immunoprecipitation (Figure 5E). Single-molecule fluorescent in situ hybridization analysis further confirmed the preferential expression of *Adrb1* mRNAs in BGCs, identified here by *Gfap* transcripts in the PC layer (Figure 5F). To evaluate the contribution β1-AR in the regulation of GluA1 phosphorylation triggered by *d*-amphetamine, C57/Bl6 mice were administered with either propranolol, a general β-AR antagonist (20 mg/kg; i.p.), or betaxolol, a selective β1-AR antagonist (20 mg/kg; i.p.) 30 min prior to the injection of *d*-amphetamine or saline (Figure 5G). As revealed by western blot analyses, *d*-amphetamine failed to increased GluA1 phosphorylation in the presence of both antagonists (Figure 5G). Altogether, these findings indicate that *d*-amphetamine-induced pS845-GluA1 in BGCs requires noradrenergic transmission and β1-AR activation.

3.5 | Repeated exposure to *d*-amphetamine and methylphenidate enhances pS845-GluA1 in BGCs through β1-AR activation

Long-term exposure to *d*-amphetamine or methylphenidate induces a variety of neuronal changes that contribute to the development of long-lasting behavioral alterations.[37,38] We next investigated whether the ability of *d*-amphetamine to trigger pS845-GluA1 was preserved following repeated exposure and, if so, whether it still relied on β1-AR activation. To address this issue, C57/Bl6 mice received saline or *d*-amphetamine (10 mg/kg) for five consecutive days. Before each administration, mice were pretreated with betaxolol (20 mg/kg) or its vehicle. The level of pS845-GluA1 was analyzed in cerebellar membrane fractions 15 min after the last injection of saline or *d*-amphetamine. Western blot analysis revealed that the ability of *d*-amphetamine to increase pS845-GluA1 in BGCs was preserved in mice repeatedly exposed to *d*-amphetamine (Figure 6A). This increased phosphorylation still relied on β1-AR activation because pS845-GluA1 was totally prevented in mice pretreated with betaxolol (Figure 6A).

We next examined whether repeated exposure to *d*-amphetamine induced transcriptional alterations of genes encoding proteins involved in the regulation of cAMP/PKA pathway turnover. To address this question, we compared by qRT-PCR the expression level of several BGCs-enriched transcripts between mice repeatedly administered with saline or *d*-amphetamine (Figures 6B and S5). Our analysis revealed a significant increase of *Adrb1* and *Acdy2* transcripts encoding β1-AR and adenylate cyclase 2 in mice exposed five consecutive days to *d*-amphetamine (Figure 6B). Conversely, the level of *Ppm1a* and *Ppp1r14c* mRNAs encoding protein phosphatase, Mg^{2+}/Mn^{2+} dependent 1A and protein phosphatase 1 regulatory subunit 14C, respectively, were reduced upon this *d*-amphetamine-treatment regimen (Figure 6B). Similar results were obtained in mice repeatedly exposed to methylphenidate, in which a decreased expression of mRNAs encoding phosphodiesterase 7B (*Pde7b*) was observed

(Figure 6C,D). Altogether, these results indicate that β1-AR-dependent GluA1 phosphorylation in BGCs is preserved in mice repeatedly exposed to *d*-amphetamine or methylphenidate. Moreover, our findings identify BGCs transcriptional alterations of several regulators of the cAMP/PKA pathway, which account for the absence of pS845-GluA1 desensitization.

4 | DISCUSSION

Our findings indicate that systemic administration of *d*-amphetamine and methylphenidate drive cAMP/PKA-regulated phosphorylation of GluA1 in BGCs. This regulation requires intact NE transmission via the activation of β1-AR. Finally, our study identified transcriptional alterations of several components of the cAMP/PKA pathway, which may account for the maintenance of the stimulant medications ability to increase GluA1 phosphorylation following drug administration.

The demonstration of a rapid and selective increase of GluA1 phosphorylation at S845 in the cerebellum following *d*-amphetamine and methylphenidate administration extend previous observations identifying similar regulatory mechanisms in other brain regions by a wide range of psychostimulants.[15,16] Our data suggest that each psychostimulant generate specific patterns of GluA1 phosphorylation, as it is the case for ERK pathway.[39] Thus, increased pS845-GluA1 in the cerebellum was not induced by cocaine but instead only observed following the administration of stimulant medications. This contrasts with the striatum, where enhanced GluA1 phosphorylation occurs in response to all psychostimulants.[15,28,29] Several reasons may account to the inability of cocaine to increase GluA1 phosphorylation. Thus, although cocaine blocks all three monoamine transporters equally well, it is much less potent in inhibiting NET than methylphenidate or *d*-amphetamine.[40] The different pharmacokinetics for the three drugs could represent another factor as well as the role played by the sigma 1 receptor in the regulation of cocaine-mediated intracellular signaling.[41] Finally, the ability of cocaine versus stimulant medications to recruit distinct monoaminergic circuits also certainly account for the specificity of GluA1 phosphorylation patterns induced by these drugs. Thus, in densely DA-innervated regions such as the striatum, psychostimulants-induced pS845-GluA1 is mediated primarily through D1R activation.[15,28,29] In contrast, our study reveals that in the cerebellum, in which both DA and NE extracellular concentrations increased following *d*-amphetamine and methylphenidate administration,[11,42] GluA1 phosphorylation relies exclusively on NE transmission via β1-AR activation, akin to the mechanism described in the prefrontal cortex.[16,43] Interestingly, hippocampal GluA1 phosphorylation, which is enhanced by *d*-amphetamine,[44] is also strongly regulated by NE and β1-AR agonist,[45,46] suggesting that the contribution of the noradrenergic system in the regulation of pS845-GluA1 by stimulant medications is certainly not restricted to the cerebellum and the prefrontal cortex.

Psychostimulant-induced pS845-GluA1 in the striatum and the prefrontal cortex occur in D1R- and β1-AR-containing neurons.[16,28,29] Our data clearly indicate that the ability of *d*-amphetamine or methylphenidate to enhance GluA1 phosphorylation is not specific to neurons but can also occur in astrocytes. In contrast to other brain regions, the expression of GluA1 subunit in the cerebellum is preferentially restricted to BGCs.[19,26] In these glial cells, GluA1–GluA4 containing AMPA receptors play an important role in regulating the astrocytic coverage of PC glutamatergic synapses.[18,20] Whether GluA1 phosphorylation at S845 in BGCs potentiates AMPA currents[13] and/or regulates surface trafficking of GluA1[47] as in neurons remains to be established. Moreover, future studies will be necessary to determine whether *d*-amphetamine-induced pS845-GluA1 in BGCs is causally linked to the long-lasting β-AR-dependent reduction of PC firing rate induced by acute and repeated *d*-amphetamine exposure.[10,48,49]

Recent evidence indicates that depending on the vigilance states, astrocytes of the auditory cortex integrate NE activity through distinct signaling pathways. Thus, while transient NE release is accompanied with large cytosolic astrocytic Ca^{2+} elevations, sustained activity of noradrenergic neurons leads to a gradual increase of cAMP.[50] Our results strongly suggest that similar regulations occur in BGCs because β1-AR-mediated GluA1 phosphorylation induced by stimulant medications relies on sustained activity on LC NE neurons projecting to the cerebellum. Despite the lack of regulation of GluA1 phosphorylation at the calcium-dependent site S831, BGCs Ca^{2+} dynamics might also be modulated in response to psychostimulants. Thus, α1-AR-dependent BGCs Ca^{2+} elevation has been reported during locomotion,[51] a behavioral response highly enhanced by *d*-amphetamine and methylphenidate exposure.[33] Moreover, acute *d*-amphetamine administration increases Ca^{2+} signaling in astrocytes in the nucleus accumbens though astrocytic D1R activation. Such regulatory mechanism is functionally important because it contributes to the modulation of both excitatory synaptic transmission and acute hyperlocomotor effects of *d*-amphetamine.[52] Although D1Rs expressed in BGCs do not participate to the regulation of GluA1 phosphorylation, their potential role in the regulation of BGCs Ca^{2+} signaling will require further investigation.

Structural and functional abnormalities in the cerebellum were among the first reported in patients diagnosed for ADHD. Thus, smaller cerebellar volumes have been frequently described, the Lobules VIII–X being particularly affected.[53–55] Importantly, the severity of ADHD symptoms correlates to the extent of cerebellar volume reduction, which can be compensated by methylphenidate treatment.[56–59] Interestingly, increased metabolic activity could be one of the mechanisms by which methylphenidate normalizes cerebellar dysfunction observed in ADHD.[60,61] Supporting this hypothesis, methylphenidate has been shown to increases glutamate uptake in BGCs contributing to normalize impaired metabolic homeostasis reported in ADHD.[62] Future studies will determine whether disruption of cerebellar glutamate homeostasis may contribute to the development of substance use disorders associated with the nonmedical use of stimulant medications.

ACKNOWLEDGEMENTS

We thank the iExplore, MRI, and PVM Platforms of the IGF for their involvement in the maintenance and breeding of the colonies. We thank Zoé Husson for her insightful comments. This work was supported by Inserm, *Fondation pour la Recherche Médicale* (DEQ20160334919), *La Marató de TV3 Fundació* (#113-2016) , ANR EPITRACES, ANR DOPAFEAR (EV), NARSAD Young Investigator Grant from the Brain and Behavior Research Foundation (E. P.), and CIHR project grant 201803PJT (B. G.). Laura Cutando is supported by the post-doctoral Labex EpiGenMed fellowship («Investissements d'avenir» ANR-10-LABX-12-01); E. P. was a recipient of Marie Curie Intra-European Fellowship IEF327648 and is currently a recipient of a *Beatriu de Pinós* fellowship (# 2017BP00132) from the University and Research Grants Management Agency (Government of Catalonia, Spain). Laia Castell is supported by the PhD Labex EpiGenMed fellowship («Investissements d'avenir» ANR-10-LABX-12-01). P. B. and A. K. E. are research associate and research director of the FRS-FNRS respectively, and both are supported by FNRS; AKE is also supported by the Foundation Simone and Pierre Clerdent.

CONFLICT OF INTEREST

The authors declare no conflicts of interest.

AUTHOR CONTRIBUTIONS

LC, EP and EV conceived, designed, and led the project. LC and EP performed brain dissections. LC and EP performed polysome IP and qRT-PCR experiments. LC and FB performed western blot analyses. LC, EP, and PT performed immunofluorescence experiments. LC and LC performed in situ hybridization analysis. MG and GD provided *Gfap-Cre*^{ERT2} mice and reagents. PB and AK performed stereotaxic injections in *Dbh-Cre* mice. VP and CL assisted with the anatomical analysis of the *Slc6a3-Cre* mouse. EI and BG generated and provided VMAT2-cKO mice. EV supervised the project. LC and EV wrote the manuscript with input from all authors.

ORCID

Laura Cutando https://orcid.org/0000-0002-0176-4550
Emma Puighermanal https://orcid.org/0000-0003-4271-9104
Laia Castell https://orcid.org/0000-0001-8755-9795
Federica Bertaso https://orcid.org/0000-0003-3140-019X
Patricia Bonnavion https://orcid.org/0000-0003-4760-2589
Alban de Kerchove d'Exaerde https://orcid.org/0000-0002-0682-5877
Elsa Isingrini https://orcid.org/0000-0002-0698-4237
Micaela Galante https://orcid.org/0000-0001-9656-9936
Glenn Dallerac https://orcid.org/0000-0002-4518-4099
Vincent Pascoli https://orcid.org/0000-0002-7130-2626
Christian Lüscher https://orcid.org/0000-0001-7917-4596
Bruno Giros https://orcid.org/0000-0001-5876-9822
Emmanuel Valjent https://orcid.org/0000-0002-1034-606X

REFERENCES

1. Wilens TE, Spencer TJ. Understanding attention-deficit/hyperactivity disorder from childhood to adulthood. *Postgrad Med*. 2010;122(5):97-109.
2. Lakhan SE, Kirchgessner A. Prescription stimulants in individuals with and without attention deficit hyperactivity disorder: misuse, cognitive impact, and adverse effects. *Brain Behav*. 2012;2(5):661-677.
3. Engert V, Pruessner JC. Dopaminergic and noradrenergic contributions to functionality in ADHD: the role of methylphenidate. *Curr Neuropharmacol*. 2008;6(4):322-328.
4. Gatley SJ, Pan D, Chen R, Chaturvedi G, Ding YS. Affinities of methylphenidate derivatives for dopamine, norepinephrine and serotonin transporters. *Life Sci*. 1996;58(12):231-239.
5. Kuczenski R, Segal DS. Effects of methylphenidate on extracellular dopamine, serotonin, and norepinephrine: comparison with amphetamine. *J Neurochem*. 1997;68(5):2032-2037.
6. Weyandt LL, Oster DR, Marraccini ME, et al. Prescription stimulant medication misuse: where are we and where do we go from here? *Exp Clin Psychopharmacol*. 2016;24(5):400-414.
7. Ikai Y, Takada M, Shinonaga Y, Mizuno N. Dopaminergic and non-dopaminergic neurons in the ventral tegmental area of the rat project, respectively, to the cerebellar cortex and deep cerebellar nuclei. *Neuroscience*. 1992;51(3):719-728.
8. Nelson TE, King JS, Bishop GA. Distribution of tyrosine hydroxylase-immunoreactive afferents to the cerebellum differs between species. *J Comp Neurol*. 1997;379(3):443-454.
9. Panagopoulos NT, Papadopoulos GC, Matsokis NA. Dopaminergic innervation and binding in the rat cerebellum. *Neurosci Lett*. 1991;130(2):208-212.
10. Freedman R, Marwaha J. Effects of acute and chronic amphetamine treatment on Purkinje neuron discharge in rat cerebellum. *J Pharmacol Exp Ther*. 1980;212(3):390-396.
11. Quansah E, Ruiz-Rodado V, Grootveld M, Zetterström TSC. Methylphenidate alters monoaminergic and metabolic pathways in the cerebellum of adolescent rats. *Eur Neuropsychopharmacol*. 2018;28(4):513-528.
12. Stoodley CJ. The cerebellum and neurodevelopmental disorders. *Cerebellum*. 2016;15(1):34-37.
13. Roche KW, O'Brien RJ, Mammen AL, Bernhardt J, Huganir RL. Characterization of multiple phosphorylation sites on the AMPA receptor GluR1 subunit. *Neuron*. 1996;16(6):1179-1188.
14. Wang JQ, Arora A, Yang L, et al. Phosphorylation of AMPA receptors: mechanisms and synaptic plasticity. *Mol Neurobiol*. 2005;32(3):237-249.
15. Mao LM, Diaz JA, Fibuch EE, Wang JQ. Regulation of phosphorylation of synaptic and extrasynaptic GluA1 AMPA receptors in the rat forebrain by amphetamine. *Eur J Pharmacol*. 2013;715(1–3):164-171.
16. Pascoli V, Valjent E, Corbillé AG, et al. cAMP and extracellular signal-regulated kinase signaling in response to *d*-amphetamine and methylphenidate in the prefrontal cortex in vivo: role of beta 1-adrenoceptors. *Mol Pharmacol*. 2005;68(2):421-429.
17. Petralia RS, Wenthold RJ. Light and electron immunocytochemical localization of AMPA-selective glutamate receptors in the rat brain. *J Comp Neurol*. 1992;318(3):329-354.
18. De Zeeuw CI, Hoogland TM. Reappraisal of Bergmann glial cells as modulators of cerebellar circuit function. *Front Cell Neurosci*. 2015;9:246.
19. Douyard J, Shen L, Huganir RL, Rubio ME. Differential neuronal and glial expression of GluR1 AMPA receptor subunit and the scaffolding proteins SAP97 and 4.1N during rat cerebellar development. *J Comp Neurol*. 2007;502(1):141-156.
20. Saab AS, Neumeyer A, Jahn HM, et al. Bergmann glial AMPA receptors are required for fine motor coordination. *Science*. 2012;337(6095):749-753.

21. Pascoli V, Terrier J, Hiver A, Lüscher C. Sufficiency of mesolimbic dopamine neuron stimulation for the progression to addiction. *Neuron*. 2015;88(5):1054-1066.
22. Franklin K, Paxinos G. *The Mouse Brain in Stereotaxic Coordinates* (3rd ed.). USA: Academic Press, Elsevier; 2008.
23. Biever A, Puighermanal E, Nishi A, et al. PKA-dependent phosphorylation of ribosomal protein S6 does not correlate with translation efficiency in striatonigral and striatopallidal medium-sized spiny neurons. *J Neurosci*. 2015;35(10):4113-4130.
24. Ozaita A, Puighermanal E, Maldonado R. Regulation of PI3K/Akt/GSK-3 pathway by cannabinoids in the brain. *J Neurochem*. 2007;102(4):1105-1114.
25. Puighermanal E, Cutando L, Boubaker-Vitre J, et al. Anatomical and molecular characterization of dopamine D1 receptor-expressing neurons of the mouse CA1 dorsal hippocampus. *Brain Struct Funct*. 2017;222(4):1897-1911.
26. Burnashev N, khodorova A, Jonas P, et al. Calcium-permeable AMPA-kainate receptors in fusiform cerebellar glial cells. *Science*. 1992;256(5063):1566-1570.
27. Koirala S, Corfas G. Identification of novel glial genes by single-cell transcriptional profiling of Bergmann glial cells from mouse cerebellum. *PLoS One*. 2010;5(2):e9198.
28. Snyder GL, Allen PB, Fienberg AA, et al. Regulation of phosphorylation of the GluR1 AMPA receptor in the neostriatum by dopamine and psychostimulants in vivo. *J Neurosci*. 2000;20(12):4480-4488.
29. Valjent E, Pascoli V, Svenningsson P, et al. Regulation of a protein phosphatase cascade allows convergent dopamine and glutamate signals to activate ERK in the striatum. *Proc Natl Acad Sci U S A*. 2005;102(2):491-496.
30. Wilens TE, Spencer TJ, Biederman J. A review of the pharmacotherapy of adults with attention-deficit/hyperactivity disorder. *J Atten Disord*. 2002;5(4):189-202.
31. Kuczenski R, Segal DS, Todd PK. Behavioral sensitization and extracellular dopamine responses to amphetamine after various treatments. *Psychopharmacology (Berl)*. 1997;134(3):221-229.
32. Camps M, Kelly PH, Palacios JM. Autoradiographic localization of dopamine D1 and D2 receptors in the brain of several mammalian species. *J Neural Transm Gen Sect*. 1990;80(2):105-127.
33. Valjent E, Bertran-Gonzalez J, Aubier B, Greengard P, Hervé D, Girault JA. Mechanisms of locomotor sensitization to drugs of abuse in a two-injection protocol. *Neuropsychopharmacology*. 2010;35(2):401-415.
34. Isingrini E, Perret L, Rainer Q, et al. Resilience to chronic stress is mediated by noradrenergic regulation of dopamine neurons. *Nat Neurosci*. 2016;19(4):560-563.
35. Gelinas JN, Tenorio G, Lemon N, Abel T, Nguyen PV. Beta-adrenergic receptor activation during distinct patterns of stimulation critically modulates the PKA-dependence of LTP in the mouse hippocampus. *Learn Mem*. 2008;15(5):281-289.
36. Doyle JP, Dougherty JD, Heiman M, et al. Application of a translational profiling approach for the comparative analysis of CNS cell types. *Cell*. 2008;135(4):749-762.
37. Kim Y, Teylan MA, Baron M, Sands A, Nairn AC, Greengard P. Methylphenidate-indued dendritic spine formation and ΔFosB expression in nucleus accumbens. *Proc Natl Acad Sci U S a*. 2009;106(8):2915-2920.
38. Sokolov BP, Polesskaya OO, Uhl GR. Mouse brain gene expression changes after acute and chronic amphetamine. *J Neurochem*. 2003;84(2):244-252.
39. Valjent E, Pagès C, Hervé D, Girault JA, Caboche J. Addictive and non-addictive drugs induce distinct and specific patterns of ERK activation in mouse brain. *Eur J Neurosci*. 2004;19(7):1826-1836.
40. Han DD, Gu HH. Comparison of the monoamine transporters from human and mouse in their sensitivities to psychostimulant drugs. *BMC Pharmacol*. 2006;6(1):6.
41. Soriani O, Kourrich S. The sigma-1 receptor: when adaptive regulation of cell electrical activity contributes to stimulant addiction and cancer. *Front Neurosci*. 2019;13:1186.
42. Krobert KA, Sutton RL, Feeney DM. Spontaneous and amphetamine-evoked release of cerebellar noradrenaline after sensorimotor cortex contusion: an in vivo microdialysis study in the awake rat. *J Neurochem*. 1994;62(6):2233-2240.
43. Xue B, Edwards MC, Mao LM, et al. Rapid and sustained GluA1 S845 phosphorylation in synaptic and extrasynaptic locations in the rat forebrain following amphetamine administration. *Neurochem Int*. 2014;64:48-54.
44. Mao LM, Xue B, Jin DZ, Wang JQ. Dynamic increases in AMPA receptor phosphorylation in the rat hippocampus in response to amphetamine. *J Neurochem*. 2015;133(6):795-805.
45. Hu H, Real E, Takamiya K, et al. Emotion enhances learning via norepinephrine regulation of AMPA-receptor trafficking. *Cell*. 2007;131(1):160-173.
46. Tenorio G, Connor SA, Guévremont D, et al. Silent' priming of translation-dependent LTP by ß-adrenergic receptors involves phosphorylation and recruitment of AMPA receptors. *Learn Mem*. 2010;17(12):627-638.
47. Serulle Y, Zhang S, Ninan I, et al. A GluR1-cGKII interaction regulates AMPA receptor trafficking. *Neuron*. 2007;56(4):670-988.
48. Sorensen SM, Hattox S, Johnson SW, Bickford P, Murphy R, Freedman R. Norepinephrine-dependent and independent mechanisms of persistent effects of amphetamine in rat cerebellum. *Life Sci*. 1985;36(25):2383-2389.
49. Sorensen SM, Johnson SW, Freedman R. Persistent effects of amphetamine on cerebellar Purkinje neurons following chronic administration. *Brain Res*. 1982;247(2):365-371.
50. Oe Y, Wang X, Patriachi T, et al. Distinct temporal integration of noradrenaline signaling by astrocytic second messengers during vigilance. *Nat Commun*. 2020;11(1):471.
51. Paukert M, Agarwal A, Cha J, Doze VA, Kang JU, Bergles DE. Norepinephrine controls astroglial responsiveness to local circuit activity. *Neuron*. 2014;82(6):1263-1270.
52. Corkrum M, Covelo A, Lines J, et al. Dopamine-evoked synaptic regulation in the nucleus accumbens requires astrocyte activity. *Neuron*. 2020;105(6):1036-1047.
53. Berquin PC, Giedd JN, Jacobsen LK, et al. Cerebellum in attention-deficit hyperactivity disorder: a morphometric MRI study. *Neurology*. 1998;50(4):1087-1093.
54. Hill DE, Yeo RA, Campbell RA, Hart B, Vigil J, Brooks W. Magnetic resonance imaging correlates of attention-deficit/hyperactivity disorder in children. *Neuropsychology*. 2003;17(3):496-506.
55. Mostofsky SH, Reiss AL, Lockhart P, Denckla MB. Evaluation of cerebellar size in attention-deficit hyperactivity disorder. *J Child Neurol*. 1998;13(9):434-439.
56. Bledsoe J, Semrud-Clikeman M, Pliszka SR. A magnetic resonance imaging study of the cerebellar vermis in chronically treated and treatment-naïve children with attention-deficit/hyperactivity disorder combined type. *Biol Psychiatry*. 2009;65(7):620-624.
57. Castellanos FX, Lee PP, Sharp W, et al. Developmental trajectories of brain volume abnormalities in children and adolescents with attention-deficit/hyperactivity disorder. *JAMA*. 2002;288(14):1740-1748.
58. Ivanov I, Murrough JW, Bansal R, Hao X, Peterson BS. Cerebellar morphology and the effects of stimulant medications in youths with attention deficit-hyperactivity disorder. *Neuropsychopharmacology*. 2014;39(3):718-726.
59. Rubia K, Halari R, Cubillo A, Mohammad AM, Brammer M, Taylor E. Methylphenidate normalises activation and functional

connectivity deficits in attention and motivation networks in medication-naïve children with ADHD during a rewarded continuous performance task. *Neuropharmacology*. 2009;57(7–8):640-652.
60. Volkow ND, Wang GJ, Fowler JS, et al. Differences in regional brain metabolic responses between single and repeated doses of methylphenidate. *Psychiatry Res*. 1998;83(1):29-36.
61. Volkow ND, Wang GJ, Fowler JS, et al. Decreased striatal dopaminergic responsiveness in detoxified cocaine-dependent subjects. *Nature*. 1997;386(6627):830-833.
62. Guillem AM, Martinez-Lozada Z, Hernandez-Kelly LC, et al. Methylphenidate increases glutamate uptake in Bergmann glial cells. *Neurochem Res*. 2015;40(11):2317-2324.

SUPPORTING INFORMATION

Additional supporting information may be found online in the Supporting Information section at the end of this article.

How to cite this article: Cutando L, Puighermanal E, Castell L, et al. Regulation of GluA1 phosphorylation by *d*-amphetamine and methylphenidate in the cerebellum. *Addiction Biology*. 2020;e12995. https://doi.org/10.1111/adb.12995